

# CALIS - a calibration insertion system for the DarkSide-50 dark matter search experiment

P. Agnes<sup>a</sup>, T. Alexander<sup>ae</sup>, A. Alton<sup>b</sup>, K. Arisaka<sup>ad</sup>, H.O. Back<sup>x</sup>,  
B. Balding<sup>g</sup>, K. Biery<sup>g</sup>, G. Bonfini<sup>q</sup>, M. Bossa<sup>i</sup>, A. Brigatti<sup>s</sup>, J. Brodsky<sup>x</sup>,  
F. Budano<sup>y</sup>, L. Cadonati<sup>ae</sup>, F. Calaprice<sup>x</sup>, N. Canci<sup>ad</sup>, A. Candela<sup>q</sup>,  
H. Cao<sup>x</sup>, M. Cariello<sup>h</sup>, P. Cavalcante<sup>q</sup>, A. Chavarria<sup>d</sup>, A. Chepurnov<sup>t</sup>,  
A.G. Cocco<sup>u</sup>, L. Crippa<sup>s</sup>, D. D'Angelo<sup>s</sup>, M. D'Incecco<sup>q</sup>, S. Davini<sup>k</sup>,  
M. De Deo<sup>q</sup>, A. Derbin<sup>v</sup>, A. Devoto<sup>c</sup>, F. Di Eusonio<sup>x</sup>, G. Di Pietro<sup>s</sup>,  
E. Edkins<sup>j</sup>, A. Empl<sup>k</sup>, A. Fan<sup>ad</sup>, G. Fiorillo<sup>u</sup>, K. Fomenko<sup>f</sup>, G. Forster<sup>ae</sup>,  
D. Franco<sup>a</sup>, F. Gabriele<sup>q</sup>, C. Galbiati<sup>x</sup>, A. Goretti<sup>x</sup>, L. Grandi<sup>d</sup>,  
M. Gromov<sup>t</sup>, M.Y. Guan<sup>l</sup>, Y. Guardincerri<sup>g</sup>, B. Hackett<sup>j</sup>, K. Herner<sup>g</sup>,  
E.V. Hungerford<sup>k</sup>, Al. Ianni<sup>q</sup>, An. Ianni<sup>x</sup>, C. Jollet<sup>aa</sup>, K. Keeter<sup>e</sup>,  
C. Kendziora<sup>g</sup>, S. Kidner<sup>af,1</sup>, V. Kobylev<sup>n</sup>, G. Koh<sup>x</sup>, D. Korablev<sup>f</sup>,  
G. Korga<sup>k</sup>, A. Kurlej<sup>ae</sup>, P.X. Li<sup>l</sup>, B. Loer<sup>x</sup>, P. Lombardi<sup>s</sup>, C. Love<sup>ab</sup>,  
L. Ludhova<sup>s</sup>, S. Luitz<sup>z</sup>, Y.Q. Ma<sup>l</sup>, I. Machulin<sup>o,r</sup>, A. Mandarano<sup>i</sup>, S. Mari<sup>y</sup>,  
J. Maricic<sup>j</sup>, L. Marini<sup>y</sup>, C.J. Martoff<sup>ab</sup>, A. Meregaglia<sup>aa</sup>, E. Meroni<sup>s</sup>,  
P.D. Meyers<sup>x,\*</sup>, R. Milincic<sup>j</sup>, D. Montanari<sup>g</sup>, A. Monte<sup>ae</sup>, M. Montuschi<sup>q</sup>,  
M.E. Monzani<sup>z</sup>, P. Mosteiro<sup>x</sup>, B. Mount<sup>e</sup>, V. Muratova<sup>v</sup>, P. Musico<sup>h</sup>,  
A. Nelson<sup>x</sup>, S. Odrowski<sup>q</sup>, M. Okounkova<sup>x</sup>, M. Orsini<sup>q</sup>, F. Ortica<sup>w</sup>,  
L. Pagani<sup>h</sup>, M. Pallavicini<sup>h</sup>, E. Pantic<sup>ad,ac</sup>, L. Papp<sup>af</sup>, S. Parmeggiano<sup>s</sup>,  
R. Parsells<sup>x</sup>, K. Pelczar<sup>m</sup>, N. Pelliccia<sup>w</sup>, S. Perasso<sup>a</sup>, A. Pocar<sup>ae</sup>,  
S. Pordes<sup>g</sup>, D. Pugachev<sup>o</sup>, H. Qian<sup>x</sup>, K. Randle<sup>ae</sup>, G. Ranucci<sup>s</sup>,  
A. Razeto<sup>q</sup>, B. Reinhold<sup>j</sup>, A. Renshaw<sup>ad</sup>, A. Romani<sup>w</sup>, B. Rossi<sup>x,u</sup>,  
N. Rossi<sup>q</sup>, S.D. Rountree<sup>af</sup>, D. Sablone<sup>k</sup>, P. Saggese<sup>q</sup>, R. Saldanha<sup>d</sup>,  
W. Sands<sup>x</sup>, S. Sangiorgio<sup>p</sup>, E. Segreto<sup>q</sup>, D. Semenov<sup>v</sup>, E. Shields<sup>x</sup>,  
M. Skorokhvatov<sup>o,r</sup>, O. Smirnov<sup>f</sup>, A. Sotnikov<sup>f</sup>, C. Stanford<sup>x</sup>,  
Y. Suvorov<sup>ad</sup>, R. Tartaglia<sup>q</sup>, J. Tatarowicz<sup>ab</sup>, G. Testera<sup>h</sup>, A. Tonazzo<sup>a</sup>,  
E. Unzhakov<sup>v</sup>, R.B. Vogelaar<sup>af</sup>, M. Wada<sup>x</sup>, S. Walker<sup>u</sup>, H. Wang<sup>ad</sup>,  
Y. Wang<sup>l</sup>, A. Watson<sup>ab</sup>, S. Westerdale<sup>x</sup>, M. Wojcik<sup>m</sup>, A. Wright<sup>x</sup>,  
X. Xiang<sup>x</sup>, J. Xu<sup>x</sup>, C.G. Yang<sup>l</sup>, J. Yoo<sup>g</sup>, S. Zavatarelli<sup>h</sup>, A. Zec<sup>ae</sup>, C. Zhu<sup>x</sup>,  
G. Zuzel<sup>lm</sup>

---

\*Corresponding authors.

Email address: meyers@princeton.edu (P.D. Meyers)

<sup>1</sup>Deceased

- <sup>a</sup>*APC, Université Paris Diderot, Sorbonne Paris Cité, Paris 75205, France*
- <sup>b</sup>*Physics and Astronomy Department, Augustana College, Sioux Falls, SD 57197, USA*
- <sup>c</sup>*Physics Department, Università degli Studi and INFN, Cagliari 09042, Italy*
- <sup>d</sup>*Kavli Institute, Enrico Fermi Institute and Dept. of Physics, University of Chicago, Chicago, IL 60637, USA*
- <sup>e</sup>*School of Natural Sciences, Black Hills State University, Spearfish, SD 57799, USA*
- <sup>f</sup>*Joint Institute for Nuclear Research, Dubna 141980, Russia*
- <sup>g</sup>*Fermi National Accelerator Laboratory, Batavia, IL 60510, USA*
- <sup>h</sup>*Physics Department, Università degli Studi and INFN, Genova 16146, Italy*
- <sup>i</sup>*Gran Sasso Science Institute, L’Aquila 67100, Italy*
- <sup>j</sup>*Department of Physics and Astronomy, University of Hawai’i, Honolulu, HI 96822, USA*
- <sup>k</sup>*Department of Physics, University of Houston, Houston, TX 77204, USA*
- <sup>l</sup>*Institute of High Energy Physics, Beijing 100049, China*
- <sup>m</sup>*Smoluchowski Institute of Physics, Jagiellonian University, Krakow 30059, Poland*
- <sup>n</sup>*Institute for Nuclear Research, National Academy of Sciences of Ukraine, Kiev 03680, Ukraine*
- <sup>o</sup>*National Research Centre Kurchatov Institute, Moscow 123182, Russia*
- <sup>p</sup>*Lawrence Livermore National Laboratory, 7000 East Avenue, Livermore, CA 94550*
- <sup>q</sup>*Laboratori Nazionali del Gran Sasso, Assergi (AQ) 67010, Italy*
- <sup>r</sup>*National Research Nuclear University MEPhI (Moscow Engineering Physics Institute), 115409 Moscow, Russia*
- <sup>s</sup>*Physics Department, Università degli Studi and INFN, Milano 20133, Italy*
- <sup>t</sup>*Skobeltsyn Institute of Nuclear Physics, Lomonosov Moscow State University, Moscow 119991, Russia*
- <sup>u</sup>*Physics Department, Università degli Studi Federico II and INFN, Napoli 80126, Italy*
- <sup>v</sup>*St. Petersburg Nuclear Physics Institute, Gatchina 188350, Russia*
- <sup>w</sup>*Chemistry, Biology and Biotechnology Department, Università degli Studi and INFN, Perugia 06123, Italy*
- <sup>x</sup>*Department of Physics, Princeton University, Princeton, NJ 08544, USA*
- <sup>y</sup>*Physics Department, Università degli Studi Roma Tre and INFN, Roma 00146, Italy*
- <sup>z</sup>*SLAC National Accelerator Laboratory, Menlo Park, CA 94025, USA*
- <sup>aa</sup>*IPHC, Université de Strasbourg, CNRS/IN2P3, Strasbourg 67037, France*
- <sup>ab</sup>*Physics Department, Temple University, Philadelphia, PA 19122, USA*
- <sup>ac</sup>*Physics Department, University of California, Davis, CA 95616, USA*
- <sup>ad</sup>*Physics and Astronomy Department, University of California, Los Angeles, CA 90095, USA*
- <sup>ae</sup>*Amherst Center for Fundamental Interactions and Physics Department, University of Massachusetts, Amherst, MA 01003, USA*
- <sup>af</sup>*Physics Department, Virginia Tech, Blacksburg, VA 24061, USA*

---

## Abstract

In order to calibrate the detector response and detection efficiency of the DarkSide-50 Liquid Argon Time Projection Chamber used for dark

matter detection and the surrounding 30 t organic liquid scintillator neutron veto, we designed, built and implemented a calibration source insertion system (CALIS), which allows to deploy radioactive sources into the liquid scintillator veto. It was commissioned in September 2014 and used successfully in several campaigns to deploy gamma and neutron sources since then.

*Keywords:*

Dark matter, WIMP, Noble liquid detectors, Low-background detectors,

Liquid scintillators, radioactive source calibration

PACS: 95.35.+d, 29.40.Mc, 29.40Gx

---

**1** **Contents**

|           |                                                                   |           |
|-----------|-------------------------------------------------------------------|-----------|
| <b>2</b>  | <b>1</b> <b>Introduction</b>                                      | <b>4</b>  |
| <b>3</b>  | <b>2</b> <b>Design Requirements &amp; Hardware Implementation</b> | <b>7</b>  |
| 4         | 2.1 Hardware . . . . .                                            | 7         |
| 5         | 2.2 Design Requirements . . . . .                                 | 10        |
| 6         | 2.3 Hardware Details . . . . .                                    | 11        |
| 7         | 2.4 Degrees of freedom of the system . . . . .                    | 14        |
| <b>8</b>  | <b>3</b> <b>Testing, Cleaning and Commissioning</b>               | <b>17</b> |
| 9         | 3.1 Commisioning and testing at LNGS . . . . .                    | 27        |
| 10        | 3.2 Proposed Commissioning Plan . . . . .                         | 30        |
| 11        | 3.3 Source arms . . . . .                                         | 30        |
| 12        | 3.4 Calibration of Z-position and Articulation Angle . . . . .    | 31        |
| 13        | 3.5 Operational Procedure . . . . .                               | 31        |
| <b>14</b> | <b>4</b> <b>Calibration Campaigns</b>                             | <b>34</b> |
| 15        | 4.1 TPC Observables and PE Calibration . . . . .                  | 34        |
| 16        | 4.2 TPC Calibration with Internal Sources . . . . .               | 34        |
| 17        | 4.3 Radioactive Sources . . . . .                                 | 36        |
| 18        | 4.4 Neutron sources . . . . .                                     | 37        |
| 19        | 4.5 Timeline of the Calibration Campaigns . . . . .               | 37        |
| <b>20</b> | <b>5</b> <b>Analysis</b>                                          | <b>38</b> |
| 21        | 5.1 TPC . . . . .                                                 | 38        |

|    |                                                              |           |
|----|--------------------------------------------------------------|-----------|
| 22 | 5.2 Liquid Scintillator Veto . . . . .                       | 41        |
| 23 | 5.3 Impact of Calibration Source Deployment on Stability and |           |
| 24 | Radioactivity in LY . . . . .                                | 42        |
| 25 | <b>6 Conclusions</b>                                         | <b>42</b> |
| 26 | <b>7 Outlook</b>                                             | <b>42</b> |
| 27 | <b>8 Epilogue</b>                                            | <b>42</b> |

## 28 **1. Introduction**

29 DarkSide-50 is a Liquid Argon Time Projection Chamber (LAr TPC),  
 30 operated in the Gran Sasso National Laboratory (LNGS) in Italy to search  
 31 for nuclear recoils induced by weakly interacting massive particles (WIMPs).  
 32 A first physics result was reported in [? ] based on 50 live days of data col-  
 33 lected with Atmospheric Argon (AAr), providing the most sensitive limit  
 34 on a dark matter search using a LAr TPC to date with a 90% CL upper  
 35 limit on the WIMP-nucleon spin-independent cross section of  $6.1 \times 10^{-44}$   
 36  $\text{cm}^2$  for a WIMP mass of 100 GeV/c<sup>2</sup>.

37 The DarkSide-50 apparatus has been described in detail in [? ], but  
 38 for the reader’s convenience a short reminder is given. As shown in  
 39 fig. 1 it features a LAr TPC surrounded by a 30 t liquid scintillator-based  
 40 veto (LSV) system, which in turn is housed in a water Cerenkov detector  
 41 (WCD), both of which help to measure in-situ and suppress radiogenic  
 42 and cosmogenic backgrounds. On top of the WCD there is a clean room  
 43 (CRH) which houses the cryogenic supply system, the electronics and  
 44 slow control software, among other things. The LSV is accessible from  
 45 CRH through four access ports nick named organ pipes which end in gate  
 46 valves. The CALibration source Insertion System (CALIS) is connected to  
 47 one of the gate valves and allows to deploy radioactive sources through  
 48 the organ pipe into the neutron veto and position it next to the cryostat  
 49 of the LAr TPC. (fig. 2, right).

50 The goal with the calibration source insertion system CALIS is to  
 51 study and calibrate the detector response of the TPC and the LSV as well  
 52 as the detection efficiency of internal neutrons interacting in the TPC and  
 53 LSV using radioactive gamma and neutron sources. The WCD in contrast  
 54 is gain calibrated only using a Laser system, which is sufficient to veto  
 55 muons (and their secondaries) with high efficiency.

56 After this introduction the CALIS design requirements and hardware  
 57 realization are described in Sec. 2. The testing, cleaning and commis-  
 58 sioning before and after the installation in CRH are outlined in Sec. ??.  
 59 Analysis results are discussed in Sec. 5, before concluding in Sec. ??

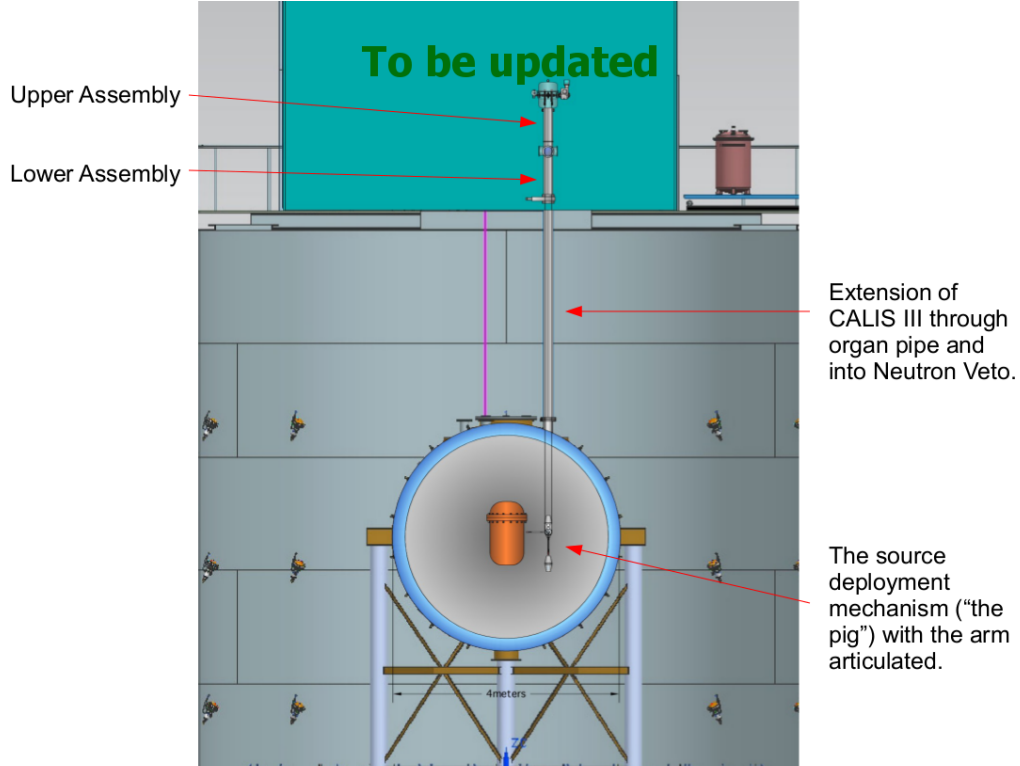


Figure 1: A conceptual drawing of CALIS installed in the radon-suppressed clean room CRH atop the water Cerenkov detector (WCD) and with the deployment device containing the source deployed in the liquid scintillator veto (LSV) next to the liquid argon time projection chamber's (LAr TPC) cryostat. The clean room and the LSV are connected through four access ports nick named organ pipes (only one of which is drawn in the sketch above: (1)). All four organ pipes end in CRH at gate valves (2) which can be manually opened or closed. During normal operations all four organ pipes are closed. Not included in the sketch are tubes connecting the cryogenic systems in CRH to the cryostat in the LSV ((3) and (4)).

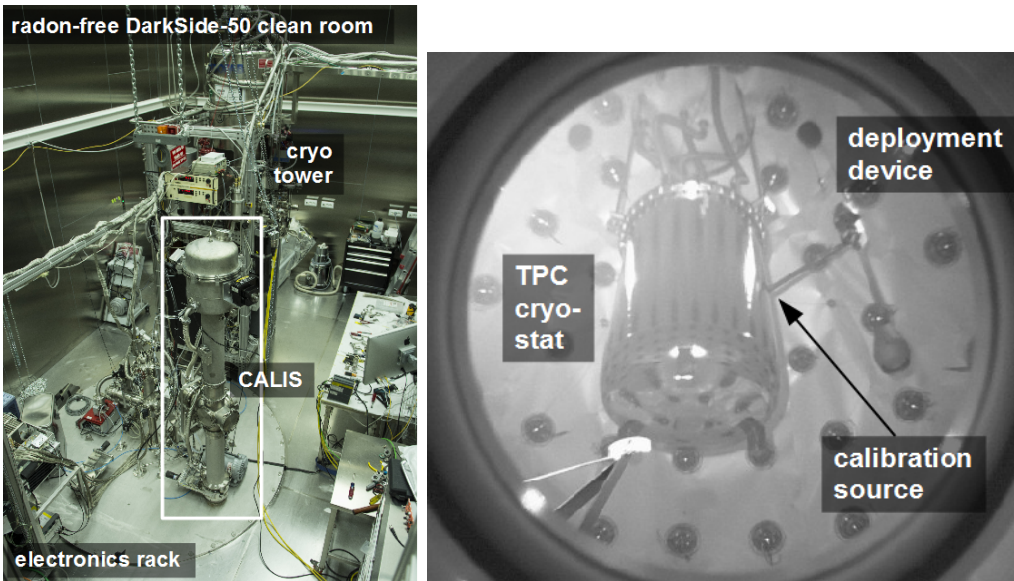


Figure 2: *left*: CALIS after installation inside the CRH room. *right*: Photograph taken with a camera looking upwards into the LSV from the bottom. It shows the source deployment device deployed through one of the organ pipes visible on the top right. The arm is articulated and the source is next to the cryostat of the LAr TPC.

60 **2. Design Requirements & Hardware Implementation**

61 *2.1. Hardware*

62 The apparatus consists of the housing, which has been installed in  
63 CRH (Fig. 2, left) and the deployment device which can be lowered into  
64 the LSV (Fig. 2, right). The deployment device is attached to the hous-  
65 ing through two stainless steel cables that are wound up on cable spools  
66 (Fig. 3).

67 *2.1.1. Deployment & Articulation*

68 The center of the LSV is about 6 m below the gate valve inside CRH  
69 and the 6" wide organ pipes are vertical, yet about 80 cm off center in  
70 the XY plane as shown in Fig. 2. For TPC calibration the radioactive  
71 source has to be positioned in immediate contact with the cryostat, in  
72 order to minimize rate losses through absorption in particular for low  
73 energy sources such as  $^{57}\text{Co}$  (122 keV). This is made possible by enabling  
74 the deployment device to articulate an arm, at whose end the radioactive  
75 source is thereby brought close the cryostat.

76 In order to send the deployment device into the LSV, both cables are  
77 unwound simultaneously. The stepper motor moves both cable spools  
78 concurrently and an absolute encoder monitors the current position of  
79 the deployment device. The stepper motor is controlled via a simple  
80 graphical LabVIEW interface, run on a dedicated laptop, in which the  
81 current z-position is shown and a target z-position can be provided by  
82 the operator. Z-positions are given in motor step counts, an arbitrary unit  
83 which has been calibrated outside CRH in meters and relative to the TPC  
84 using calibration data.

85 Articulation of the arm is done manually via the articulation wheel  
86 (Fig. 3). This affects only the cable spool close to the articulation wheel,  
87 the left one in Fig. 3, thereby shortening the left cable wrt. to the right  
88 cable and engaging the gear through a chain (Fig. 4). As a result the arm  
89 is articulated and the pivot center is lifted. The degrees corresponding to  
90 a horizontal articulation has been calibrated prior to installation in CRH  
91 (Sec. ??).

92 Articulation and a movement in z-direction are mutually exclusive  
93 since the articulation of the arm leads to more wound up cable on the  
94 spool close to the articulation wheel wrt. the other. If then in deploy-  
95 ment mode both spools would be rotated simultaneously with the same

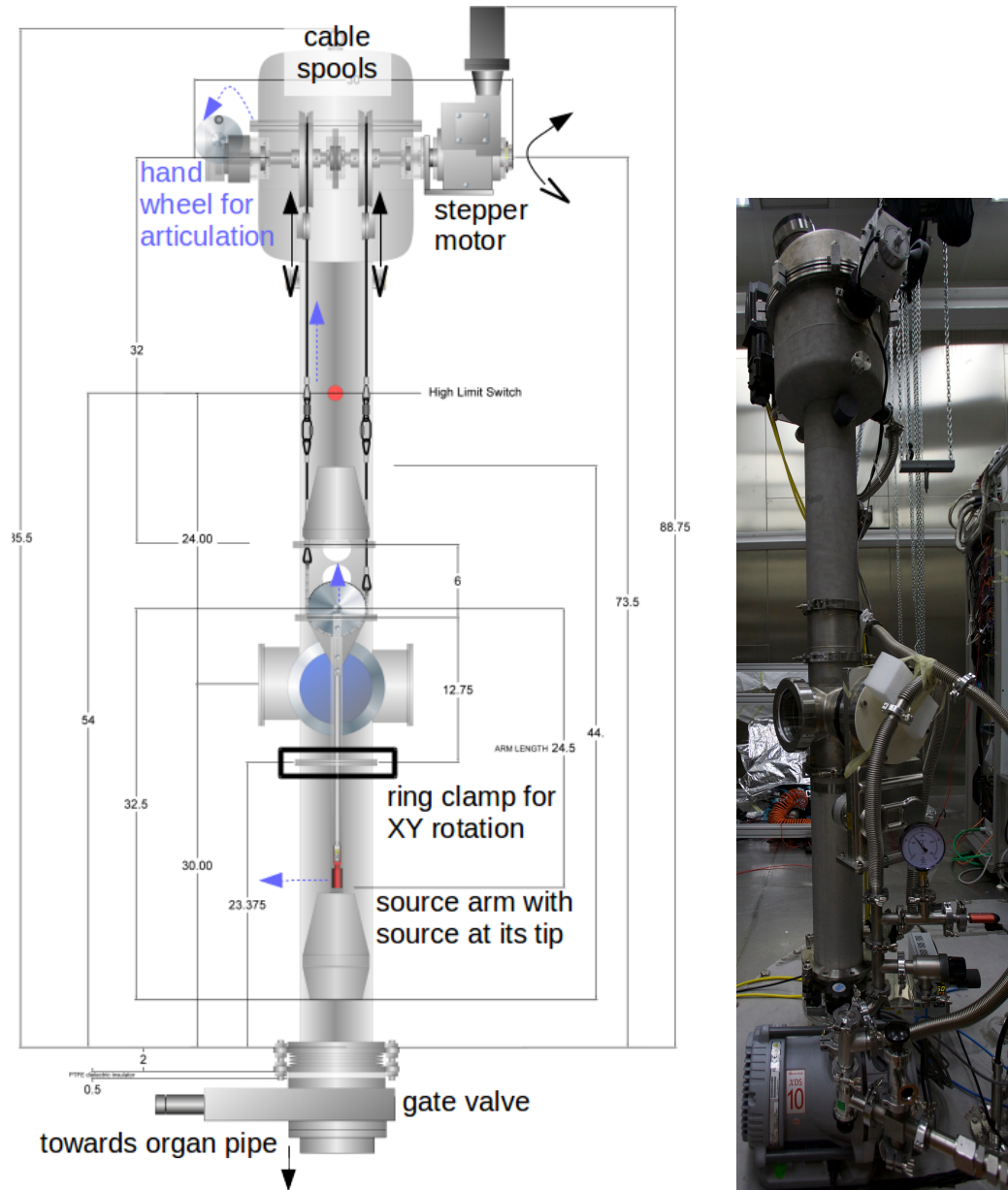


Figure 3: Mechanical drawing of CALIS showing the housing and the deployment device. Dimensions are in inches. (The total height of 88.75 inches corresponds to 225.425 cm.) The two modes of operation are illustrated: In order to move the deployment device down into the LSV or back up the stepper motor moves both cable spools simultaneously. In order to articulate, the articulation wheel is rotated manually, which affects only the left spool, thereby shortening the left cable wrt. to the right cable thereby articulating the arm and lifting the pivot center. The amount of lifting and the amount of rotations until a horizontal articulation is reached has been calibrated prior to installation in CRH (Sec. ??)

96 angular speed, the cable close to the articulation wheel would wind up  
 97 faster than the other, which would lead to a build up of difference in cable  
 98 length and the deployment device would only be hanging on one cable.  
 99 In order to avoid an imbalanced z-movement the arm has to be dearticu-  
 100 lated before a change in z-position can be initiated. This is enforced by an  
 101 electric switch preventing z-movement, which is disengaged only when  
 102 the arm is fully dearticulated.

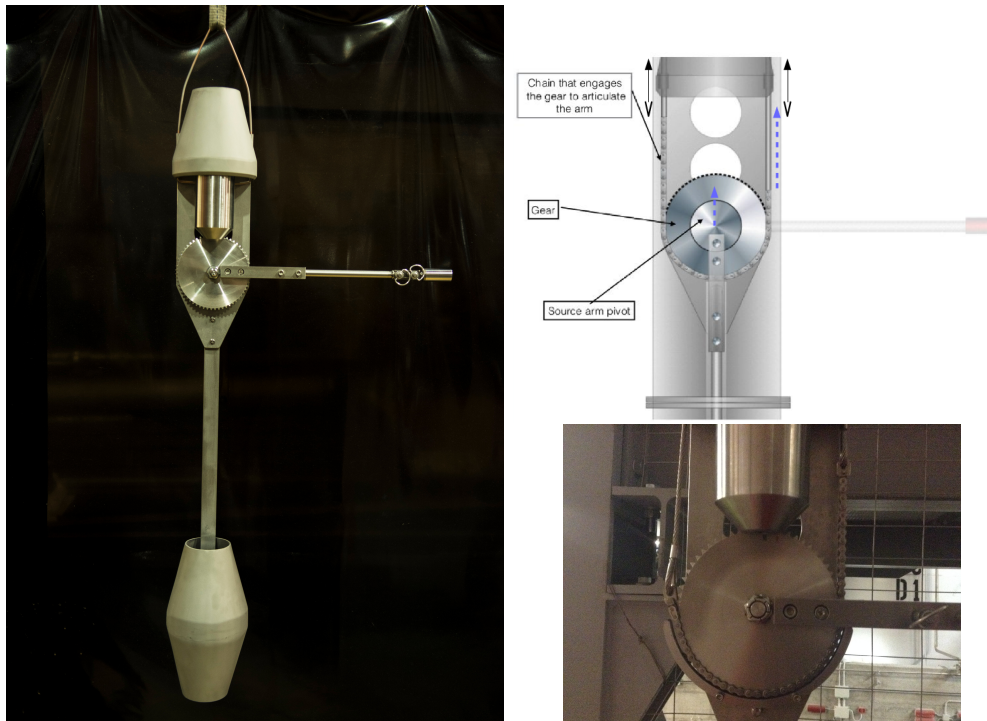


Figure 4: Technical drawing showing the articulation mechanism using a chain that engages the gear to transfer the rotation of the articulation wheel (Fig. 3) into a rotation of the source arm. The chain has a guard rail, not shown in the drawing, that ensures that the chain can never come off the gear.

103 *2.1.2. Housing & Scintillator*

104 Besides providing mechanical support for the deployment device, the  
 105 housing is the important interface between CRH and the LSV, through  
 106 which sources are exchanged, while protecting the liquid scintillator and  
 107 avoiding human contact with the liquid scintillator. The liquid scintil-

108 lator, which is a mixture of PC and TMB<sup>2</sup> with the wavelength shifter  
109 PPO[? ], may not get exposed to oxygen or water as is present in normal  
110 clean room air and also contamination with  $^{222}\text{Rn}$  and its daughters has  
111 to be avoided. Vacuum and nitrogen pressurization systems have been  
112 developed ??.

113 On the other hand TMB vapors and residues could form ...

114 *ToDo: more precise on risks of contact of TMB with air/ water. What are the  
115 dangers compared to a PC only scintillator?*

116 The housing thereby has the same role as glove boxes in calibration  
117 devices of other experiments (see e.g. [? ?]).

118 *2.2. Design Requirements*

119 The design of CALIS is shaped by the following requirements, thereby  
120 following the design principle of “form follows function”:

- 121 • to allow source exchanges and safely deploy them at various posi-  
122 tions inside the LSV,
- 123 • protecting the scintillator from oxygen and water at any time, in  
124 particular during deployments and being able to articulate a source  
125 arm in order to bring the source next to the cryostat. Also pro-  
126 tection and safety mechanisms that avoid exposure of personal to  
127 scintillators are in place.
- 128 • To complement studies of nuclear recoils with neutron sources ( $^{241}\text{Am}^9\text{Be}$   
129 and  $^{241}\text{Am}^{13}\text{C}$ ), it is planned to deploy a neutron gun inside a ded-  
130 icated deployment device currently under development (Section 7).
- 131 • All materials that come in contact with the scintillator veto are made  
132 of stainless steel and teflon except for the sealing o-rings which are  
133 made out of viton. All three materials (stainless steel, teflon, and  
134 viton) are certified materials for contact with TMB and PC.
- 135 • Before assembly in CRH, each component of CALIS, the ones intro-  
136 duced into the scintillator as well as those in the clean room CRH,  
137 have been subjected to the official cleaning procedure [? ].

138 This results in further hardware design choices and requirements that  
139 are discussed below.

---

<sup>2</sup>As discussed in Sec. ?? the concentration of TMB has varied during the campaigns.

140    2.3. *Hardware Details*

141    2.3.1. *Housing*

142    Here the design of the housing shown in fig. 3 is described in more  
143    detail. Starting at the gate valve inside the clean room CRH on which  
144    CALIS has been installed, a teflon disk allows to electrically isolate  
145    CALIS from ground, even though during normal operations the CALIS  
146    housing is also connected to ground. A tripod with a bellow has been  
147    used to vertically align the housing right after installation on the gate  
148    valve. The bellow is connected to a 23.375" long cylindrical stainless steel  
149    enclosure pipe. It has the same diameter as the organ pipe (6") and leads  
150    into a view port (depicted in blue in fig. 3) and which is the access point  
151    for accessing the source arm and exchanging sources.

152    Above the view port is the upper assembly, which is a stainless steel  
153    cylindrical enclosure that houses the cable drive mechanism, including  
154    the cable spools the stepper motor and the articulation mechanism, al-  
155    ready described in Sec. 2.1.1.

156    CALIS offers various safety features to ensure that the device runs  
157    smoothly, no components are lost inside the detector, avoid any contam-  
158    ination of the detector by dirty or incompatible materials, maintain pres-  
159    sure and avoid introduction of oxygen or water in contact with the LS  
160    and TMB, operation in the volume that excludes possibility of contact  
161    with PMTs or light pulsers (pacman) attached to each PMT.

162    2.3.2. *Safety features*

163    **Drive mechanism:** The drive mechanism is a stepper motor that has an  
164    integrated absolute encoder providing the location of the source at  
165    all times, even in the event of a power failure. In the event of a  
166    power failure, the magnetic break ensures there is no movement  
167    of the pig. The torque of the servo motor is limited in case of an  
168    unexpected load.

169    The speed reducer (gears) is a double worm gear design. The pri-  
170    mary worm gear has a 50:1 reduction and the secondary worm has  
171    a 82:1 reduction. The input speed of the servo motor is 2400 RPMs  
172    and the output is 0.6 RPM and has the weight capacity of 148 lbs. In  
173    the event of a power failure the speed reducer has the ability to hold  
174    the load at any position without back drive. The speed of the motor  
175    has been limited to 0.4 cm/s which minimizes any lateral oscillation

176 of the pig during lowering and raising the source. Additionally, this  
177 is the maximum speed at which the motor is not overheating.

178 **Manual retraction system:** In the unlikely case of a complete motor fail-  
179 ure while the source is deployed, it is possible to manually retract  
180 the pig back to its home position and close the gate valve. The mo-  
181 tor is disengaged, and wrench is used to manually wind the cable  
182 back onthe spools and retract the pig back above the gate valve.

183 **Cable strength and length:** The cables holding the pig have been rated  
184 for loads over 590 kg, while the weight of the pig is at the level of  
185 10-15 kg so well below the breaking strength of the cable. The cable  
186 length has been established so that the maximum depth at which the  
187 pig can be deployed is above the level of the PMTs inside the LSV.  
188 In case, the command is given to deploy to greater depth, the cable  
189 completely unwinds and then rewinds in the opposite direction,  
190 which then effectively retracts the pig to a higher z-position until  
191 the preset motor count of steps is reached.

192 **Upper limit switch:** The motor has an absolute encoder and step posi-  
193 tion is never lost even in the case when the motor loses power. When  
194 the pig has reached its home position within the upper assembly it  
195 will stop. However, if the top of the pig continues past its home  
196 position (based on the number of steps given), it will not be able to  
197 pass its home position thanks to the upper limit switch that will be  
198 triggered in that case.

199 Neither the manual retraction system has been used nor has the  
200 upper limit switch been activated during calibration campaigns.

201 **Light and leak tightness of CALIS:** When the deployment device is next  
202 to the cryostat the gate valve is open and we take also data with the  
203 LSV. A prerequisite is that the housing is absolute light tight and  
204 pressure leak tight. All view ports have light tight covers for when  
205 the organ pipe gate valve is open. Both light and leak tightness has  
206 been extensively validated throughout the manufacturing process  
207 until including commissioning (Sec. 3).

### 208 2.3.3. Deployment device

209 The pig (Fig. ??) contains the support structure for the arm which  
210 holds the source at its end. This piece is equipped with tapered cones on

211 the top and bottom that ensure that the ends do not get snagged on inner  
212 edges of the organ pipe as it is moving up and down. It is attached to  
213 the housing by two cables. Swivel hooks are employed in the attachment  
214 of the cables to the pig that allow the cables to move freely and not get  
215 tangled. There are two weights built into the device, one cylindrical in the  
216 conical cap above the rotation gear mechanism and one inside the cones  
217 at the bottom end of the device. Both help to minimize any lateral motion  
218 or oscillations during deployment and articulation and dearticulation es-  
219 pecially. It also ensures smooth motion of the deployment device into the  
220 organ pipe and back to the home position inside the housing.

221 *2.3.4. Source holder and arms*

222 A source arm and the source holder are attached to the articulation  
223 gear (Fig. 5). Different arm lengths have been prepared with a maximum  
224 arm length of 62 cm, the arm length thereby being measured from the  
225 pivot point of the rotation gear to the tip of the source holder. This arm  
226 length allows the source to be placed in immediate contact with the cryo-  
227 stat (Fig. 2, right), as the center axis of the organ pipe is 81 cm from the  
228 TPC center and the cryostat has an outer radius of 32 cm. The 62 cm  
229 arm was used for most of the deployments in the past calibration cam-  
230 paigns (Sec. ??). Inside the source holder the radioactive source is placed,  
231 pressed to the tip and held in place via a spring during deployment, ar-  
232 tication and dearticulation. The source holder is sealed such that no  
233 liquid scintillator can enter during the deployment. This has also been  
234 verified during each source extraction, that no liquid was found on the  
235 inside.

236 *2.3.5. Securing of the source*

237 All connection points for the source and arm have been secured with  
238 two push locking pins that cannot be disengaged without a person press-  
239 ing the pin. The source holder is held in place via a locking mechanism  
240 and two locking pins. When the source is attached to the arm, the source  
241 container must be slid over a protruding pin. There is a sliding locking  
242 mechanism that interlocks onto the pin. Once the source is locked into  
243 position there are 2 additional locking pins that are put into place (one  
244 above and one below the source holder pin), each of which have a button  
245 that must be depressed in order for the pins to be released. In addition,  
246 the source holder and the 2 locking pins will all be tethered from outside



Figure 5: Source holder that connects to an arm and to the articulation gear of the deployment device. The source, here a  $^{133}\text{Ba}$  source is pressed to the tip of the source holder via a spring.

247 the view port until they are locked in place eliminating the possibility  
 248 of accidental falling. The tethering will happen before installation of the  
 249 source and before the removal of the source. The cables used to tether the  
 250 pins and the source holder during installation and removal will be de-  
 251 tached after installation and prior to deployment to avoid the possibility  
 252 of the arm getting entangled.

#### 253 2.4. Degrees of freedom of the system

254 CALIS has the capability to deploy sources at various positions inside  
 255 the LSV. Besides the movement along z up to the maximum cable length,  
 256 there is the possibility to articulate at an angle of  $\theta$  between  $90^\circ$  and  $180^\circ$ ,  
 257 where  $\theta$  is the zenith-angle (Fig. 6). Degrees between  $0^\circ$  and  $90^\circ$  are  
 258 excluded because the end of the articulation chain is reached at an angle  
 259 of  $90^\circ$  (see Fig. 4).

##### 260 2.4.1. Rotation in the XY plane

261 Below the view port is a sealed connection that has an o-ring seal  
 262 and uses a ring clamp to compress the seal. The clamp can be slightly  
 263 loosened to allow the assembly above and including the view port to be  
 264 rotated with respect to the lower assembly and the detector. This rotation  
 265 in the XY plane can even be performed while the gate valve is opened  
 266 and the deployment device is deployed next to the cryostat, since the seal  
 267 is helium leak and light tight even when loosened.

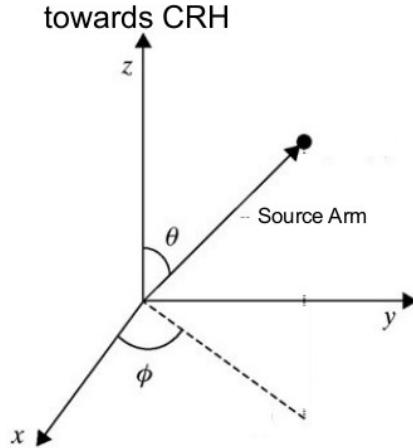


Figure 6: Spherical coordinate system used for establishing the direction of the rotation of CALIS-III and the articulation of the source arm.  $\theta$  is kept at  $90^\circ$  when arm is articulated, and at  $180^\circ$  when dearticulated.  $x$ -axis is the direction toward the center of the detector.

268 In principle a rotation in  $360^\circ$  can be done, except when the arm  
 269 would interfere with the cryostat. This has been used in one of the cali-  
 270 bration campaigns to deploy a neutron source directly next to the cryostat  
 271 and rotated away by  $90^\circ$  in order to study optical shadowing effects from  
 272 the cryostat (Sec. ??).

273 **2.4.2. "No fly" zone**

274 Right above the cryostat where there are many supply tubes for the  
 275 TPC a "no fly" zone has been defined. In this region no part of the  
 276 deployment device may enter, in particular not the source arm.

277 **2.4.3. Default configuration**

278 By default the deployment device has been deployed with the longest  
 279 arm (62 cm), at the center of the active volume of the TPC, with the arm  
 280 rotated in the XY plane until contact with the cryostat has been made.  
 281 Further details are provided in Sec. ??.

282 Other degrees of freedom could involve shorter arm lengths, while  
 283 longer arm lengths have been discussed but would require hardware  
 284 modifications to the deployment device. Out of a total of four organ  
 285 pipes a second one would be available for source calibration. A change  
 286 in organ pipe would require a bigger effort involving also the crane in  
 287 order to dismount CALIS and reinstall it on the other organ pipe. The

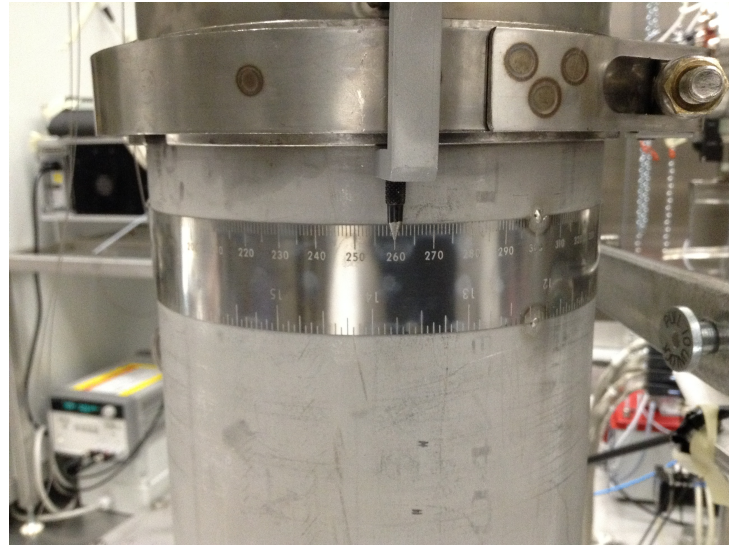


Figure 7: Ring clamp with the angle measuring strip shown below. In order to perform azimuthal rotation, the ring clamp is slightly loosened, and the entire upper assembly is rotated with respect to the lower assembly, along with the deployment device. The angle of rotation is read out from the strip that goes around the pipe. The strip is in mm, which has then been calibrated in degrees.

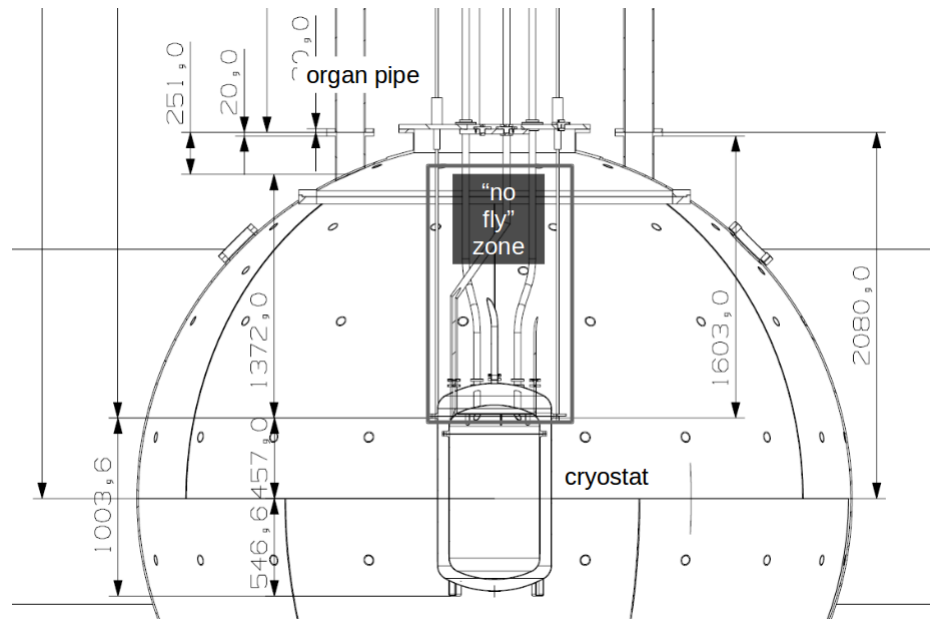


Figure 8: “No fly” zone for the CALIS source arm.

288 remaining two pipes are too close to the cryo tower or reserved for the  
289 SABRE experiment [? ].

290 Finally CALIS is designed to house also a different deployment device,  
291 such as currently being planned for the neutron gun [? ].

### 292 **3. Testing, Cleaning and Commissioning**

293 Testing of CALIS has been performed at FNAL in the second half  
294 of August and first half of September 2014. CALIS was installed in a  
295 building with the high bay, on a high platform, so that the full length  
296 deployment tests could be performed. The tests are repeated at LNGS  
297 prior to cleaning the system, and some validation tests are foreseen at the  
298 time of installation in CRH. Several different tests have been conducted:

- 299 • Light covers on the view ports Light tightness of the whole system  
300 All viewports have very tightly fitting covers. Additionally, the main  
301 viewport cover will additionally be held in place with clamps to  
302 avoid any possibility of accidentally exposing the LSV to excessive  
303 amount of light.

- 304 • Motor controls debugging

305 LabView interface with the motor controls has been verified and re-  
306 sponds to all commands (starting/stopping of vertical deployment)  
307 as expected. Motor current can be read from the GUI and shows  
308 opposite signs if motor is rotating in one vs the other direction as  
309 an additional sign of the motion direction.

- 310 • **Vertical (z) position accuracy and repeatability Procedure:** As a

311 first step in testing the reproducibility of the z position as a function  
312 of step position, a baseline relationship between step number and  
313 vertical displacement was determined. First, the distance from the  
314 floor to the bottom of the pig was measured using a laser ranger,  
315 starting from what was found to be the lowest pig position (fully  
316 deployed). The bottom of the pig was covered with tape to serve as  
317 a target for the laser ranger. After this

318 first measurement, the pig was raised, stopping approximately once  
319 every minute to record the step position and measure the corre-  
320 sponding z distance, until it reached the home position (fully re-  
321 tracted). Subsequently, in the following test runs, the pig was again

322 sent to each of these steps, the z position was measured with the  
323 laser ranger, and all values recorded. After 2 runs in which every  
324 step which had been recorded in the baseline was measured, it was  
325 realized that recording so many data points would require several  
326 weeks to complete the testing. The number of data points was then  
327 cut in half for 4 runs, and cut in half again for the remaining 24 runs  
328 for a total of 31 runs.

329 **Results:** The vertical displacement of the pig was found to be ex-  
330 tremely consistent, with no apparent drift due to slippage or any  
331 other effect. The average uncertainty of each z coordinate was found  
332 to range between 1-2 mm, numbers consistent with the uncertainty  
333 of the laser ranger and the unevenness of the tape on the bottom  
334 of the pig. Fig. 9 shows the correspondence between the z position  
335 and stepper motor count exhibiting a smooth function with no visi-  
336 ble variation of the points from the fit. No measurable slippage of  
337 the cables or accumulated offset of the stepper motor count and z  
338 position was observed during the repeated tests.

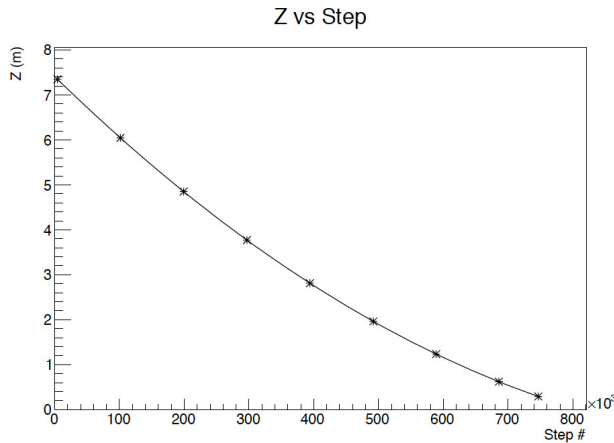


Figure 9: Plot of the z position of the pig vs the step position of the motor.

339 **• Lateral motion during deployment**

340 The pig is deployed at a very low speed, barely visible to the naked  
341 eye. It takes about 30 minutes to deploy the system from its home  
342 position to the level of the TPC, approximately 7 m below. As a  
343 result, there is a negligible level of lateral motion during vertical

344 motion at the level of 2-3 mm. The motor has a very slow acceleration  
345 (both positive and negative) that eliminates any visible jitter at  
346 the beginning or at the end of the motion.

347 **• Articulation tests**

348 **Procedure:** Arm is articulated using a manually operated hand  
349 wheel. The arm is articulated to 90° every time. This corresponds  
350 to a different reading of the dial connected to the hand wheel for  
351 different z-position. The second calibration table required, gives  
352 correspondence between the z height and required reading on the  
353 dial to articulate to 90°.

354 In order to verify the consistency of articulating to the same rotation  
355 angle of 90° at all needed positions, full articulation of the arm at  
356 different z positions was tested. For this test at Fermi lab, two vertical  
357 positions were chosen: one approximately at the center of the  
358 cryostat mock-up, and one at the lowest known position of the pig.  
359 At each position, the arm was articulated and the required angle  
360 recorded. In order to ensure that the arm was fully articulated, a  
361 level was placed on the arm and required to be horizontal. Additionally,  
362 the vertical displacement of the pig was measured before  
363 articulating the arm, while the arm was articulated and after the  
364 arm was again vertical. Between runs, the pig was sent all the way  
365 back to the home position to simulate the actual deployment conditions  
366 as closely as possible. The process was repeated 10 times (10  
367 runs) to check consistency of articulation among independent runs.

368 **Results:** During driving the pig up and down through the whole  
369 length of the cable, it was noticed that the arm did not return to a  
370 perfectly vertical position, which was especially noticeable when the  
371 pig was in the home position. To document this, photos were taken  
372 each time the arm was de-articulated and when it was in the home  
373 position. The hand wheel was renormalized to zero several times,  
374 but this offset continued to reappear. It did not seem to progress,  
375 however, and remained at approximately the same angle, as can be  
376 seen from the photographs in Fig. 10, Fig. 11, Fig. 12 and Fig. 13.  
377 In all tested cases, offset was relatively small and did not create a  
378 problem for retracting the pig inside the lower assembly pipe and  
379 to the home position.

380 It was noted that some of this offset was due to the fact that the  
381 pig is allowed to swing freely. When articulating the arm, one cable  
382 on one side of the pig is raised. This causes the pig to also slightly  
383 move in the direction of the articulation. After the arm is dearticulated,  
384 the arm returned to vertical according to the hand wheel,  
385 but not according to visual inspection and use of a level. Part of  
386 the offset is because the pig moved in the direction of articulation  
387 and during dearticulation it did not return to its original position.  
388 It seemed to get stuck at a slight offset, but a small tap on the side  
389 of the pig returned it to its original position. Additionally, the full  
390 arm articulation did not occur at exactly the same angle each time.  
391 This was most noticeable in the lowest pig position, which had an  
392 uncertainty of  $\pm 2^\circ$  (as measured on the hand crank). While searching  
393 for the cause of this, it was discovered that a portion of the cable  
394 had been stretched during earlier load testing (cable was put under  
395 300 kg load to test the strength of the crimp connections), which  
396 may have led to a slightly uneven extension / retraction of the cables,  
397 as well as tension at certain points along the line. The cable  
398 was unwound from the spool and allowed to return to its original  
399 length. The source arm had less of an offset in the vertical position  
400 than it had before adjusting the cable, although it was not perfectly  
401 straight. The articulation angle as read on the hand crank remained  
402 approximately the same. This test will be completely repeated at  
403 LNGS with the final length of the cable in question.

404 • **Magnitude of horizontal swing during articulation**

405 **Procedure:** To measure the horizontal swing of the system during  
406 articulation, a 'ruler' was devised and attached to a mock-up of  
407 the cryostat, with a smallest unit of measure of 0.6 cm. The pig  
408 was then sent to the step position where the ruler could be utilized.  
409 While the arm was articulated and de-articulated, video was taken  
410 of the swing of the pig.

411 **Results:** Analysis of the video shows that the pig swings approxi-  
412 mately 1.5 cm during articulation. The articulation is very slow and  
413 the swing is very slow. It takes a couple of minutes for the arm to  
414 come to complete rest.

415 • Electrical contact test for purpose of determining position of cryo-



Figure 10: Image of the pig in the home position. The offset of the arm is clearly visible, but below the level that creates problem for motion inside the organ pipe.



Figure 11: Another image of the pig in the home position, this time looking down into the lower assembly. Again, note the offset of the arm.



Figure 12: Image of the pig next to the cryostat mock-up and the ruler used in the horizontal swing test. Note the offset of the arm.



Figure 13: Again, the pig next to the cryostat mock-up and ruler, a close-up of the arm offset.

416 stat within the neutron veto

417 • **Procedure:** One of the main goals of the

418 first deployment of CALIS-III is to determine the location of the  
419 cryostat within the neutron veto as there is a 3-5 cm positioning  
420 uncertainty from construction in the xy-plane and 2 cm in the z di-  
421 rection.

422 One test to confirm the position of the cryostat is to electrically con-  
423 nect an arm of the pig to the cryostat. At Fermilab, the electrical  
424 contact test was simulated to prove the validity of the idea. The pig  
425 was

426 fitted with a special arm comprised of a stainless steel tube, and  
427 the cryostat mock-up received a stainless steel block attached to it  
428 via screws. At the top of CALIS-III, a wire was connected between  
429 the lower assembly and the output of a voltmeter. A wire from  
430 the stainless steel block was connected to the voltmeter input. The  
431 special arm was

432 first articulated and then the whole assembly was rotated in the  
433 azimuthal direction in order for the arm to make contact with the  
434 stainless steel block as can be seen in the Fig. 14.

435 **Results:** When the arm made contact with the square, the com-  
436 pleted circuit was indicated by the voltmeter. Contact of the arm  
437 with the steel block was also verified by visual inspection. The rota-  
438 tion and contact was repeated several times and at each contact, the  
439 voltmeter registered (by beeping) the connection.

440 • **Functionality of the safety features**

441 Both the upper limit switch and the arm retraction switch have been  
442 tested and operated as expected.

- 443 – The pig did not move above the home position, despite the  
444 command to move up in z as the power was cut to the motor.  
445 – No z-movement was possible prior to retraction of the arm to  
446 the vertical position by the hand wheel. We verify that the arm  
447 is vertical by verifying that the dial on the protractor next to  
448 the hand wheel is pointing at zero mark.

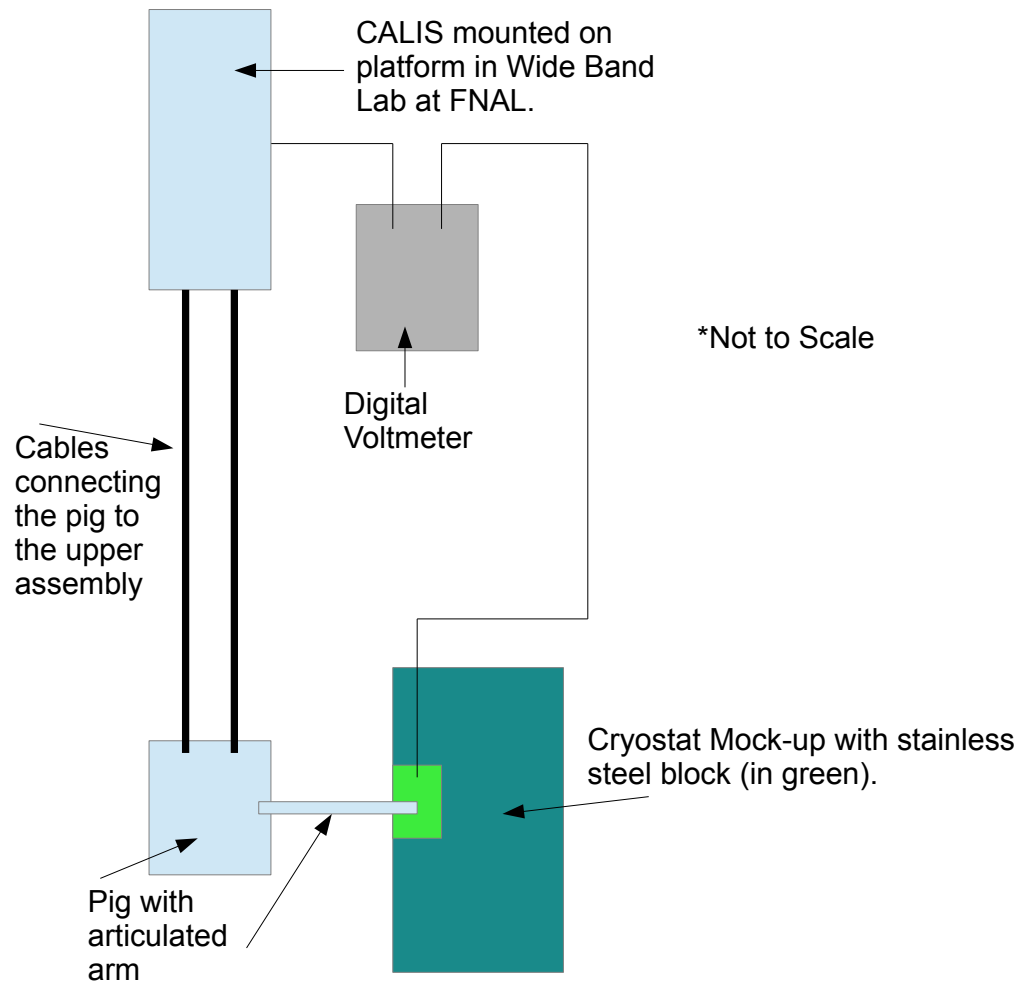


Figure 14: Diagram of the electrical contact test performed at FNAL.

449 • Test Ease and Accuracy of Azimuthal Rotation

450       **Procedure:** The upper and lower assemblies of CALIS-III can be ro-  
451       tated in the azimuthal direction. This rotation allows the source arm  
452       to move in the xy plane for the purpose of locating the position of  
453       the cryostat within the neutron veto. The rotation needs to be fairly  
454       easy to perform and we need to know what kind of precision and  
455       accuracy we will have. The rotation of the upper assembly requires  
456       one to loosen the clamp between the upper and lower assembly.  
457       Once this is done, the upper assembly is manually moved/twisted  
458       on its axis in the direction desired. To test this at Fermilab, the pig  
459       was deployed to the level of the cryostat mock-up and the arm ar-  
460       ticulated. Then the clamp was loosened and the upper assembly  
461       rotated.

462       **Results:** Despite its substantial weight, the upper assembly was able  
463       to be moved on its axis smoothly, with no jerking or sticking. At the  
464       conclusion of testing, a band was axed to the lower assembly and a  
465       pointer to the band was attached to the upper assembly. This is to  
466       measure the actual rotation of the assembly. Due to time constraints,  
467       the rotation with the band attached was not able to be done. There-  
468       fore further testing will need to be done at LNGS to determine the  
469       accuracy and precision of the azimuthal rotation.

470 • Helium Leak Tight Testing

471       The device was tested to be helium leak tight at Fermilab.

472       . A full summary, along with plots, of the testing performed at Fermilab  
473       can be found in DocDB #858.

474       After the above described tests at FNAL were finished, it was con-  
475       cluded that **CALIS is in a good operating state** and is ready to be shipped  
476       to LNGS for commissioning and calibration.

477       *3.1. Commissioning and testing at LNGS*

478       The system was shipped sub-assembled to LNGS and arrived in mid-  
479       September. Once it arrived, CALIS III was inspected and reassembled.  
480       Two rounds of tests are part of the commissioning of CALIS at LNGS:  
481       dry tests prior to cleaning and a subset of tests after cleaning the system  
482       and prior to installation on the gate valve of CRH. While the goal of the

483 Fermi lab tests was to establish that CALIS is operating as expected and  
484 that all designed safety features are operational, a goal of the LNGS tests  
485 is the final characterization of CALIS to establish the absolute positioning  
486 precision of the source.

487 The testing location chosen at LNGS allowed full deployment length  
488 tests and direct access to both the top of the system where the controls are  
489 and to the pig. The chosen location was a tall stairway on the left side of  
490 the OPERA detector that has a platform on the fourth floor where CALIS  
491 was mounted. A movable platform accessible from the lab floor level was  
492 used to raise up to the level of the pig for all planned measurements. The  
493 same set of tests as described above, and a few additional once related to  
494 the absolute positioning uncertainty, have been underway.

495 Final characterization of the source positioning must be done with  
496 the new cables that have been put on CALIS. The length of the cables  
497 was chosen to allow maximum safe, deployment depth that makes any  
498 contact with PMTs impossible (according to the engineering drawings of  
499 the DarkSide detectors). Once all dry runs are performed to satisfaction,  
500 we will disassemble and clean all components in CR1 as per the normal  
501 detector cleaning procedure. After cleaning, the device will be partially  
502 assembled and moved into CRH. A subset of validation tests will be con-  
503 ducted from the crane in the CRH and then CALIS will be installed on  
504 the top of one of the ate valves.

### 505 3.1.1. *Dry Tests to Perform at LNGS Prior to Cleaning*

506 All the tests performed at Fermilab are repeated at LNGS, but the  
507 number of runs is reduced as we do not expect to see change in the  
508 performance of the motor or the cables. While the tests at Fermi lab con-  
509 firmed good operational performance of the system, the tests conducted  
510 at LNGS are calibration tests whose goal is to make the most precise pre-  
511 diction of the source position during deployment and establish expected  
512 uncertainty of that position. Below is the full list of tests underway at  
513 LNGS.

#### 514 • Characterization of CALIS-III Positioning

515 The CALIS-III positioning has been characterized with the final ca-  
516 bles length. There are two components of the positioning:

- 517 – This includes the pig z position as a function of step position.

- 518
- 519
- The arm 90 degree articulation point as a function of vertical pig position.

520 This is necessary because, as the cable winds around the spool,  
521 the winding radius changes, increasing as the pig is lifted and de-  
522 creasing as it is lowered. This means that there is not a linear  
523 correspondence between the number of steps and the length of ca-  
524 ble deployed. Additionally, this non-linear dependency causes the  
525 amount of rotation required by the hand wheel for full articulation  
526 of the source arm to change as a function of the length of cable  
527 deployed.

528 . Every 10,000 steps (order of 10 cm), we stop the pig and record  
529 the z position with the laser ranger, as done during the position re-  
530 producibility test at Fermilab. The arm will then be rotated to 90°  
531 and the hand wheel position noted for the relevant z locations. The  
532 step position for key source locations commonly used during cali-  
533 bration will be determined, including the TPC center, 15 cm above  
534 and below the TPC center, and the cryostat top and bottom. Once  
535 these positions have been verified by inputting the step location and  
536 measuring the z position and corresponding hand wheel rotation,  
537 the results will be formatted for easy use by CALIS-III operators.

- 538
- 539
- 540
- Measure the exact distance of the forward motion (in the direction of articulation) at relevant z positions, as it determines the final distance of the source to the TPC.

541

542

543

544

  - Measure if there is any lateral change (in the azimuthal plane) when the arm is articulated at relevant z positions. While none has been observed in the previous tests, it is important to verify this in repeated deployments and articulations.

545

546

547

  - Validate the distance that the pig moves up during articulation (measured to be 10 cm in tests at Fermilab) and verify that this number does not change between repeated articulations.

548

549

  - Test the arm retraction switch to confirm that the pig cannot be retracted to its home position if the arm is articulated.

- 550     ● During articulation measure the level of the horizontal swing. Con-  
 551       firm it to agree with Fermilab testing.
- 552     ● Determine the time it takes for the arm to reach a stable (non-  
 553       moving) condition after articulation.
- 554     ● Test the absolute encoder before and after power failure.
- 555     ● Test nitrogen and vacuum systems. Measure the amount of time to  
 556       evacuate the device and purge with nitrogen.
- 557     ● Leak check of upper and lower assemblies.
- 558     ● Reproducibility of position in x, y, and z following the full proce-  
 559       dure.

560     3.1.2. *Tests to be Performed at LNGS after Cleaning*

561       After cleaning of the system, we will attach CALIS-III to a crane either  
 562       in CR1 or CRH to perform a reduced set of tests. The goal is to confirm  
 563       that results from tests prior to cleaning and from after cleaning match.

564     3.2. *Proposed Commissioning Plan*

565       Detailed, step by step commissioning procedure is outlined in DocDB#1021-  
 566       v1. Once all preliminary deployments are completed, we will continue  
 567       with the cryostat positioning and calibration campaign as outlined in  
 568       DocDB #977 for the neutron campaign, DocDB #978 for the gamma cam-  
 569       paign, and DocDB #960 – a spreadsheet dedicated to the full campaign.

570     3.3. *Source arms*

571       *My impression is that a drawing to scale with the cryostat, the TPCthe organ  
 572       pipe and the source arm would be good here*

573       For articulation, there is currently a choice of three arm lengths—  
 574       40.31 cm, 57.15 cm and 62 cm.

575       Drawing of the arm with the

576       Each of these lengths are measured from the center line of the organ  
 577       pipe to the end of the source holder. The arm lengths, 57.15 cm and 62 cm  
 578       are intentionally made too long as they will be used to determine the  
 579       exact location of the cryostat; some uncertainty in the cryostat's z and  
 580       lateral position exist at the level of 3 - 4 cm. The organ pipe we intend

581 to use is 81 cm distant from the cryostat center (and the geometric center  
582 of the LSV sphere) as measured from the center line of the organ pipe.  
583 The cryostat is 32 cm in radius, which leaves a distance of  $\sim$ 49 cm to  
584 be reached by the arm. The articulation of the arm is operated via a  
585 hand wheel located on the side of the upper assembly close to the top.  
586 By rotating the hand wheel, one of the cable spools inside the upper  
587 assembly will rotate which pulls up on one of the cables attached to the  
588 pig and shortens it for the length equal to the one quarter of the gear  
589 curcamference (which is 10 cm). As a result, the chain at the bottom of  
590 the cables engages the articulation gear (see Fig. ?? for an image of the  
591 articulation gear) on the pig and raises the arm to horizontal. The chain  
592 has a guard rail that ensures that chain can never come off the gear. Thus,  
593 in the process of articulation the entire pig along with the source arm  
594 shifts up for 10 cm. See Fig. ?? and Fig. 4 for a closer look at how CALIS  
595 III articulates the arm. In order to determine the degree of articulation of  
596 the arm, a protractor is placed next to the hand wheel. This protractor  
597 and the hand wheel are calibrated together for an accurate reading of the  
598 articulation. The reading of the protractor dial is different at different  
599 heights and calibration table obtained from the tests is used to determine  
600 the dial setting necessary to articulate the arm to horizontal position. We  
601 have adopted a spherical coordinate system for the rotation of the system  
602 and the articulation. Articulation of the arm is measured in  $\theta$  from the  
603 z-axis; when the arm is fully articulated, it is at  $90^\circ$  and when it is in  
604 its vertical position it is at  $180^\circ$ . As mentioned in Sec. ??, the rotation  
605 of CALIS III is done in the xy-plane which corresponds to the azimuthal  
606 direction, a rotation in  $\phi$ . See Fig. 6 for details.

607 3.4. *Calibration of Z-position and Articulation Angle*

608 3.5. *Operational Procedure*

609 After the testing and commissioning CALIS has been installed inside  
610 CRH...

611 Well, there also have been test deployments before that.

612 3.5.1. *Source Insertion*

613 3.5.2. *3 special positions*

614 home position or parking position - gate valve closed. The  
615 center of the TPC.

616 Full extension position - length of the cable.

617    3.5.3. *Vacuum evacuation (flushing) and nitrogen purging*

618    One of the most important features of this system is making sure that  
619    the TMB and PC residue on the device are extracted from CALIS III prior  
620    to opening access ports to exchange source or arms. This is important for  
621    safe working level of the people involved and for the detector. This can be  
622    addressed through a system evacuation and nitrogen purge. To accelerate  
623    the removal of the TMB in the scintillator fluid residue that is left after a  
624    deployment, CALIS III will undergo an evacuation with a vacuum pump.  
625    By lowering the pressure inside of CALIS below the vapor pressure of  
626    the TMB, it will cause the TMB to outgas and be removed through the  
627    vent line of the vacuum pump. An additional step to remove the TMB  
628    is to purge using N<sub>2</sub>. We will need to limit the potential flow rate of the  
629    nitrogen to ensure that an ODH (Oxygen Deficiency Hazard) condition  
630    is avoided in CRH. Only once this is accomplished, will the view port be  
631    allowed to be opened and the source handled.

632    The entire CALIS III has been tested at FNAL to hold pressure. The  
633    system will be tested again after installation on the gate valve.

634    *Opening the Gate Valve.*

635    3.5.4. *Positioning of Source*

636    *Contact with Cryostat.*

637    *Cameras.*

638    3.5.5. *Source Retraction and Extraction*

639    The source may not get in contact with the liquid scintillator. It is  
640    therefore sealed during the deployment in a dedicated source holder. In  
641    order to exchange sources the source arm and source holder has to be  
642    extracted from the pig into CRH and thereby comes in contact with nor-  
643    mal air, containing oxygen and traces of water. After insertion a flush &  
644    purge cycle is used to reduce, as known from glove boxes. No glove box  
645    present. Much more compact design.

646    After each deployment check that there is no leakage of Scintillator  
647    inside the source holder.

648    for what is helium leak tightness necessary? What was tested for  
649    helium leak tightness.

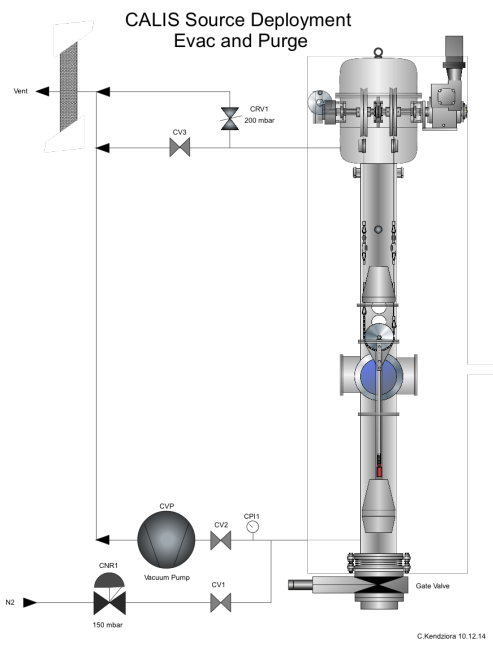


Figure 15: flushing and nitrogen purging system.

650 **4. Calibration Campaigns**

651 *4.1. TPC Observables and PE Calibration*

652 For physics analysis in the TPC the following observables have to be  
653 calibrated<sup>3</sup>:

- 654 • the scintillation signal S1,  
655 • the ionization signal S2,  
656 • the pulse shape discriminant F90,  
657 • and the position information about a given event, namely the  $t_{drift}$   
658 variable, which encodes the event's Z-position and the XY-coordinates  
659 as is reconstructed from the relative fractions of S2 signal in the top  
660 PMT array [? ].  
661 • There are also derived variables such as the top-bottom asymmetry  
662 of S1, which are used in physics analyses, but need no independent  
663 calibration beyond the underlying variable.

664 Both S1 and S2 are calibrated in photo-electrons (PE), which is done  
665 in dedicated Laser calibration runs, in which the single PE charge spectra  
666 for each PMT are fitted and a PE-charge gain is determined.

667 These Laser runs are also an integral part of a calibration campaign  
668 requiring a Laser run at least on each change in DAQ or CALIS configura-  
669 tion, such as drift field changes or source position changes.

670 *4.2. TPC Calibration with Internal Sources*

671 Prior to the insertion of external radioactive sources via CALIS the  
672 TPC could be calibrated using the  $^{39}\text{Ar}$   $\beta$ -spectrum (end point 565 keV)  
673 and by injecting a  $^{83m}\text{Kr}$  into the Ar recirculation system<sup>4</sup>. These data  
674 sets have been used for a wide range of calibrations, including light yield,  
675 electron lifetime, position reconstruction, and tuning of the optics of the  
676 DarkSide-50 Geant-4 based Monte Carlo, called G4DS [? ]. With the  
677 filling of the Underground Argon [? ],  $^{39}\text{Ar}$  is not a dominant background

---

<sup>3</sup>ToDo: Has PE already been introduced?

<sup>4</sup> $^{83m}\text{Kr}$  emits two conversion electrons at 32.1 keV and 9.1 keV, where the latter follows  
the former with a time constant of 154 ns [? ].

678 anymore and can therefore not be used for calibration, instead gamma  
 679 peaks from internal background, like  $^{60}\text{Co}$  originating in the cryostat, are  
 680 being exploited to monitor the stability of the LY.

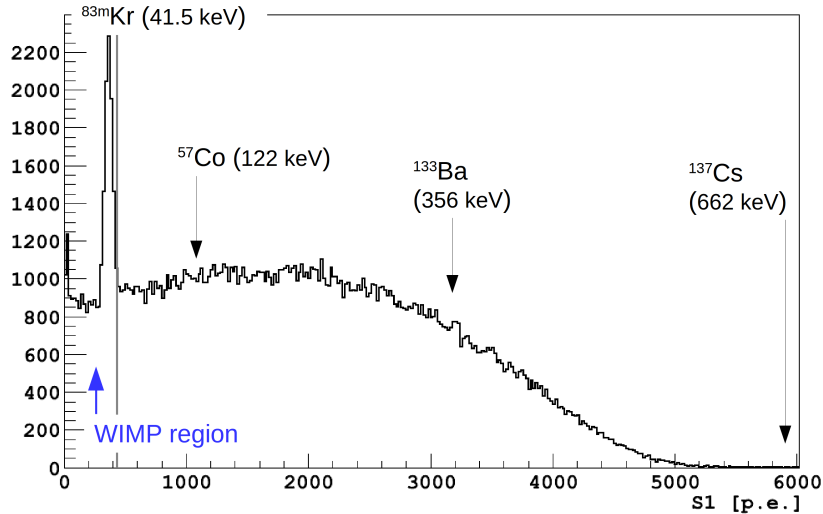


Figure 16: Scintillation spectrum ( $S_1$ ) at null field showing a  $^{83m}\text{Kr}$  peak on the  $^{39}\text{Ar}$   $\beta$  spectrum. The energies of the three gamma sources are indicated and cover the full range of the  $^{39}\text{Ar}$  spectrum.

681 *DarkSide-50 Monte Carlo*

682 G4DS is a Geant-4 based ab-initio simulation of the energy deposits  
 683 of each type of particle in LAr and in the materials building the detector,  
 684 the generation of scintillation signals, and the light collection [? ].  
 685 Specific effort has been directed toward the accurate description of the  
 686 materials and geometry of the entire detector (including the vetoes), the  
 687 tuning of all the optical parameters affecting the photon propagation, and  
 688 the development of the LAr scintillation and ionization model. The poor  
 689 experimental and theoretical constraints on electron-ion recombination  
 690 in LAr obliged us to develop our own ad-hoc effective model. The functional  
 691 form of the recombination probability was based on literature data,  
 692 and parameter values were fit to make the full MC agree with the high  
 693 statistics  $^{39}\text{Ar}$  spectrum measured in DarkSide-50. The overall photoelectron  
 694 yield of the MC was normalized at the  $^{39}\text{Ar}$  endpoint. The entire  
 695 Monte Carlo chain was then tested with the external calibration sources,  
 696  $^{57}\text{Co}$ ,  $^{133}\text{Ba}$  and  $^{137}\text{Cs}$ .

697 *4.3. Radioactive Sources*

698 For the calibration of the TPC's electron recoil (ER) response we se-  
699 lected  $^{57}\text{Co}$ ,  $^{133}\text{Ba}$  and  $^{137}\text{Cs}$  to cross calibrate with the internal  $^{39}\text{Ar}$ ,  
700 i.e. cover the full  $\beta$  spectrum (see Table 1 and Fig. 16). While all gamma  
701 sources enter the TPC active volume from outside, thanks to increasing  
702 interaction lengths as a function of energy the higher energy sources al-  
703 low to cover larger fractions of the active volume. This allows to test  
704 the detector response (S1 and S2) as well XY reconstruction in different  
705 detector areas.

706 *this interaction length argument is a bit unclear, maybe even wrong! Bernd,*  
707 *June 24th*

708 For LSV calibration the gamma sources allow to study the LY as a  
709 function of energy in close proximity to the cryostat, which is a particu-  
710 larly critical detector region for neutron backgrounds originating in the  
711 TPC itself [22]. This can be cross checked with internal backgrounds: The  
712 C14 spectrum (beta spectrum with end point at ...) in the liquid scintilla-  
713 tor of the LSV and  $^{60}\text{Co}$  originating in the cryostat steel (Sec. 5.2 and [?]  
714 ]).

Table 1: gamma sources

| source            | energy  | half life | interact. length in LAr | activity <sup>5</sup> |
|-------------------|---------|-----------|-------------------------|-----------------------|
| $^{57}\text{Co}$  | 122 keV | 0.744 y   | 4.4 cm                  | 35 kBq                |
| $^{133}\text{Ba}$ | 356 keV | 10.54 y   | 7.5 cm                  | 2 kBq                 |
| $^{137}\text{Cs}$ | 662 keV | 30.2 y    | 9.5 cm                  | 0.65 kBq              |

715 *4.3.1. Source Rate Optimization*

716 After a preselection of gamma source energies, detailed studies with  
717 the DarkSide Monte Carlo G4DS were performed to select appropriate  
718 source activities and check the feasibility and physics reach of various  
719 deployment positions.

720 On the low activity end there is the necessity to gain sufficient statis-  
721 tics and a good signal/background ratio in the presence of nearly 50 Hz  
722 of trigger rate from  $^{39}\text{Ar}$ . On the high activity end the activity is con-  
723 strained by the requirement that event pile-up fraction is limited to a  
724 few percent, which is achieved by aiming at a source induced trigger rate  
725 of about 100 Bq in the TPC. Due to the different energies and different

726 attenuation lengths of the various sources this results in significantly dif-  
727 ferent source activity requirements. For  $^{57}\text{Co}$  ( $^{137}\text{Cs}$ ) we used the source  
728 with the highest (lowest) activity available in the LNGS radioactive source  
729 repository [? ], while for the  $^{133}\text{Ba}$  all sources available at LNGS would  
730 have had a very high pile-up probability, instead a source with an activity  
731 of 1  $\mu\text{Ci}$  at 1972 was procured from Temple radio safety [? ].

732 Depending on different detector configurations, such as different drift  
733 field strengths, the DAQ can handle different trigger rates. Final adjust-  
734 ments of the source+ $^{39}\text{Ar}$  rate to a manageable trigger rate were made by  
735 prescaling the whole energy spectrum.

#### 736 4.4. Neutron sources

737 Unlike with  $^{39}\text{Ar}$  for ER there is by design very small neutron back-  
738 ground which could be used for NR calibration, which is instead pro-  
739 vided by the neutron source data, see Sec. 5.1.3). The analysis of neutron  
740 source data is heavily MC supported and so a realistic description of the  
741 detector components between the source and the active volume is an im-  
742 portant factor when studying data-MC discrepancies. Here the gamma  
743 sources provide important input as well.

744 Two AmBe sources have been deployed, a high activity source with a  
745 nominal activity of 2000 neutrons/s and a low activity source (10 n/s).  
746 With the high activity source a high statistics sample of neutrons inter-  
747 acting in the TPC has been gathered, while with the low activity source  
748 TPC-LSV coincidences and the study of the veto efficiency for nuclear  
749 recoils can be investigated. Due to PC only scintillator with a neutron  
750 capture time constant of ???<sup>6</sup>, this study was not possible with the high  
751 activity source due to event pile-up.

#### 752 4.5. Timeline of the Calibration Campaigns

753 Two calibration campaigns have been performed:

- 754 • The first extensive campaign involving all gamma sources and both  
755 the high and low activity AmBe neutron source took place in Octo-  
756 ber and November 2014 at LNGS<sup>7</sup>. The TPC was filled with atmo-  
757 spheric argon<sup>8</sup> with an inherent trigger rate of nearly 50 Hz from

---

<sup>6</sup>DocDB ???

<sup>7</sup>has LNGS been introduced?

<sup>8</sup>has atmospheric argon been introduced and underground argon?

758       <sup>39</sup>Ar. The liquid scintillator of the LSV contained a PC only scintillator  
759       with < 0.1% TMB and 1.5 g/l PPO as wavelength shifter. Fig. ??  
760       shows the different configurations in which data has been taken as  
761       a function of source energy, source position and drift field.

- 762       • In January and February 2015 a second campaign focusing on the  
763       LSV calibration using the low activity AmBe source was performed.  
764       Prior to that the LSV has been reconstituted with 5 % TMB<sup>9</sup>. Two  
765       deployments were performed at two different PPO concentrations  
766       (0.7 g/l and 1.5 g/l), allowing to study the impact of the PPO con-  
767       centration on alpha and gamma quenching. 1.5 g/l is our nominal  
768       PPO concentration.
- 769       • All external radioactive source calibrations so far have been done  
770       with the TPC filled with atmospheric argon. An underground argon  
771       calibration campaign is planned for summer 2015 (Sec. 7).

772       

## 5. Analysis

773       

### 5.1. TPC

774       

#### 5.1.1. <sup>57</sup>Co S1 energy

775       Fig. 17 shows a comparison of the scintillation signal S1 spectrum of  
776       a <sup>57</sup>Co calibration source data deployed next to the cryostat and close to  
777       the TPC active volume center. Overlayed is the S1 distribution from an  
778       equivalent selection of G4DS MC simulation. Besides passing basic cuts  
779       like baseline found or all electronics channels present, the events were  
780       restricted to single-site interactions having one S1 and one S2 pulse, also  
781       the <sup>39</sup>Ar background has been subtracted statistically. In the MC instead  
782       of an electronics simulation a clustering algorithm has been applied, that  
783       groups individual energy deposits and sums up the corresponding num-  
784       ber of PE. A single-cluster cut has been applied to correspond to single-  
785       site interactions. The <sup>57</sup>Co gamma ray spectrum (122 keV) reaching the  
786       TPC is significantly distorted by having to pass through the stainless steel  
787       source holder, outer and inner cryostat and the copper field cage rings be-  
788       fore reaching the TPC's active volume. These effects are accounted for by

---

<sup>9</sup>what does 5 % TMB mean? weight %, volume %?

789 the MC even though refinements in the material description will further  
 790 improve the already encouraging data-MC agreement.

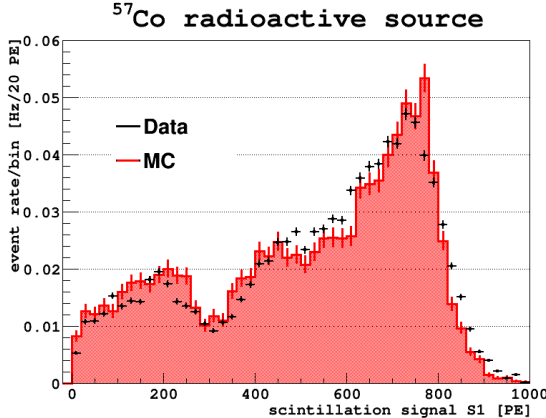


Figure 17: Data-MC comparison for the  $^{57}\text{Co}$  source deployed next to the cryostat. While some improvements are yet to be made, the level of agreement between the simulation and the various complex features of the data is very encouraging.

### 791 5.1.2. position distributions

792 The  $t_{drift}$  distribution of  $^{57}\text{Co}$  in Fig. 18 is the same run set and event  
 793 selection as for the S1 spectrum in Fig. 17. It nicely illustrates the impact  
 794 that the field rings have on the distribution. Fig. 19 shows XY distri-  
 795 butions of  $^{133}\text{Ba}$  and  $^{137}\text{Cs}$  sources deployed touching the cryostat from  
 796 the left and right, respectively, exemplarily out of a pool of possible XY  
 797 distributions.

### 798 5.1.3. $^{241}\text{Am}^9\text{Be}$ neutron data

799 The WIMP search box and nuclear recoil acceptance in our paper [?]  
 800 ] were established without the availability of neutron calibration data in  
 801 DarkSide-50. The mean F90 from the ScENE experiment [26] was scaled  
 802 to the light yield of DarkSide-50, and the electron and nuclear recoil ac-  
 803 ceptance curves were determined from an analytic statistical model of  
 804 the F90 distributions as a function of energy. While we have full confi-  
 805 dence in this approach, the data taken in the calibration campaign with  
 806 the Am-Be neutron source now allow it to be directly verified. The mean  
 807 F90 for nuclear recoils in DarkSide-50 is found to agree closely with the  
 808 corresponding scaled ScENE results, as shown in Fig. 20, right). (The

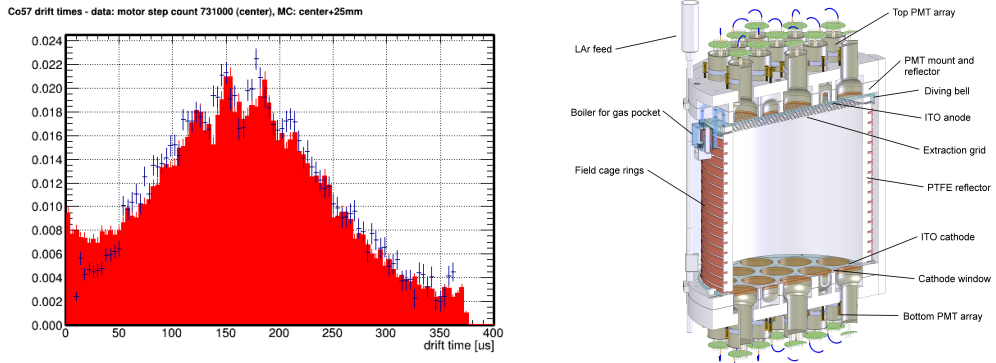


Figure 18: *left*: Data-MC comparison for the  $t_{drift}$  distribution of the  $^{57}\text{Co}$  source deployed next to the cryostat and close to the active volume center. *right*: Schematics of the TPC (without inner and outer cryostat) showing in particular the field rings, that cause a characteristic wave in the  $t_{drift}$  spectrum of  $^{57}\text{Co}$ , which is also reproduced in MC (left) [? ].

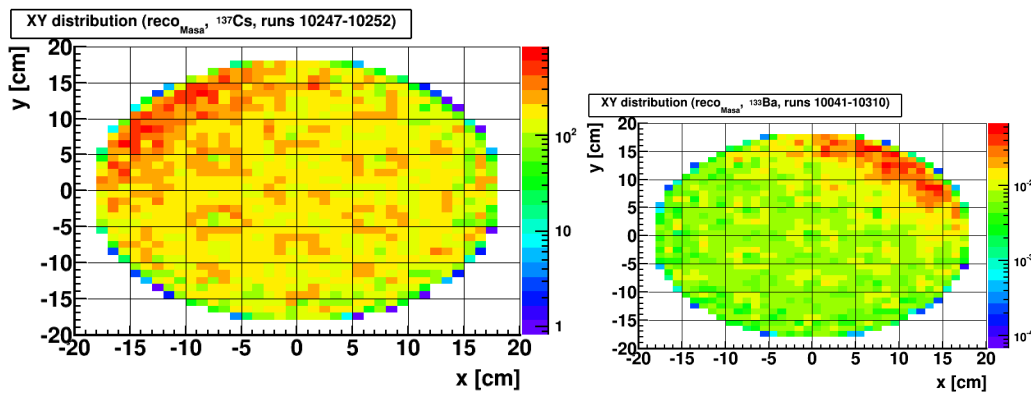


Figure 19: Two examples of XY distributions of  $^{137}\text{Cs}$  (left) and  $^{133}\text{Ba}$  (right) calibration source runs with the sources touching the cryostat from the left ( $^{137}\text{Cs}$ ) and right ( $^{133}\text{Ba}$ ). The  $^{39}\text{Ar}$  background is not subtracted and fills the TPC uniformly.

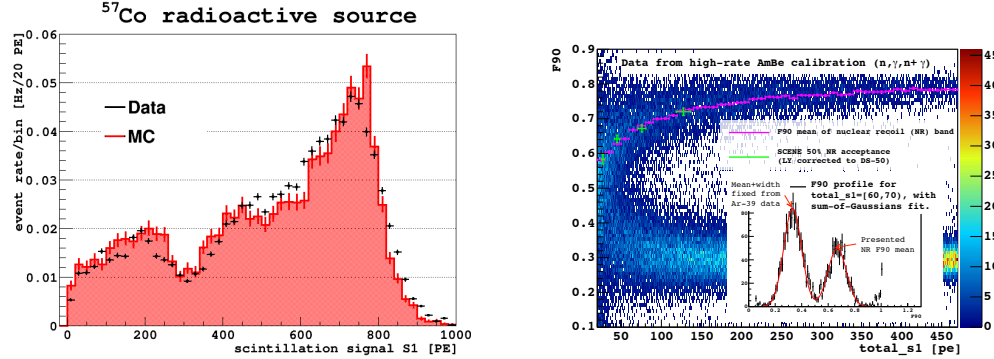


Figure 20: *left*: Data-MC comparison for the  $^{57}\text{Co}$  source deployed next to the cryostat. While some improvements are yet to be made, the level of agreement between the simulation and the various complex features of the data is very encouraging. *right*: Plot of F90 vs. scintillation signal S1 from a high rate AmBe neutron source calibration of DarkSide-50. The pink line shows the mean F90 for the nuclear recoil band, while the points in green show the F90 values scaled from SCENE measurements and used in our publication Ref. [? ]. There is very good agreement between the two. The high source intensity and correlated neutrons and  $\gamma$ -ray emission by the AmBe source contribute events outside the nuclear recoil and electron recoil bands.

higher-than-optimal intensity of this AmBe source and its correlated neutron and gamma ray emissions contribute events in the plot outside the nuclear recoil and electron recoil bands.)

#### 5.1.4. Z and XY of source position

Tests at LNGS established the deployment system's positioning accuracy to be about  $\pm 1$  cm after a 7 meter journey into the DarkSide-50 detector.

This result is being validated using calibration campaign data in an ongoing analysis.

#### 5.2. Liquid Scintillator Veto

In January and February 2015 the reconstitution of the LSV scintillator was completed and a second AmBe neutron source calibration of the LSV calibration was undertaken to further study the various neutron detection channels in the LSV. With a borated scintillator, a critical aspect of the neutron detection efficiency is the capability to observe the 6.4 % capture branch leading to a 1775 keV  $\alpha + ^7\text{Li}(\text{g.s.})$  without the accompanying 478 keV  $\gamma$ -ray. Veto results are described in further detail below in Sec. ??.

826 5.3. *Impact of Calibration Source Deployment on Stability and Radioactivity in*  
827 *LY*

828 **6. Conclusions**

829 **7. Outlook**

830 here mention the neutron gun and maybe refer to the next generation  
831 DS-detector.

832 **8. Epilogue**

833 here I would list all upcoming DarkSide papers and how they are in  
834 relationship with each other. Since so many papers are in preparation I  
835 would find that helpful. Even if it is not eventually put into the paper.

836 [1] S.M. Faber and J.S. Gallagher, [Ann. Rev. Astron. Astroph. 17, 135 \(1979\)](#).

838 [2] D.N. Spergel et al., [Ap. J. Supp. 148, 175 \(2003\)](#).

839 [3] Committee on Elementary Particle Physics in the 21st Century of the  
840 National Academies of Science, *Revealing the Hidden Nature of Space*  
841 *and Time: Charting the Course for Elementary Particle Physics*, Page 118,  
842 National Academies Press, Washington, DC (2006).

843 [4] M.W. Goodman and E. Witten, [Phys. Rev. D 31, 3059 \(1985\)](#).

844 [5] P. Benetti et al. (WARP Collaboration), [Astropart. Phys. 28, 495 \(2008\)](#).

846 [6] T. Alexander et al. (DarkSide Collaboration), [Astropart. Phys. 49, 44 \(2013\)](#).

848 [7] H.O. Back et al., [arxiv:1204.6024](#).

849 [8] H.O. Back et al., [arxiv:1204.6061](#).

850 [9] H.H. Loosli, [Earth Plan. Sci. Lett. 63, 51 \(1983\)](#).

851 [10] P. Benetti et al. (WARP Collaboration), [Nucl. Inst. Meth. A 574, 83 \(2007\)](#).

- 853 [11] J. Xu et al., *Astropart. Phys.* **66**, 53 (2015).
- 854 [12] G. Alimonti et al. (Borexino Collaboration), *Astropart. Phys.* **8**, 141  
855 (1998).
- 856 [13] G. Alimonti et al. (Borexino Collaboration), *Nucl. Instr. Meth. A* **406**,  
857 411 (1998).
- 858 [14] G. Bellini et al. (Borexino Collaboration), *JCAP* **1308**, 049 (2013).
- 859 [15] G. Alimonti et al. (Borexino Collaboration), *Nucl. Instr. Meth. A* **600**,  
860 568 (2009).
- 861 [16] G. Alimonti et al. (Borexino Collaboration), *Nucl. Instr. Meth. A* **609**,  
862 58 (2009).
- 863 [17] M. G. Boulay and A. Hime, *Astropart. Phys.* **25**, 179 (2006).
- 864 [18] G. Bellini et al. (Borexino Collaboration), *Phys. Rev. Lett.* **107**, 141302  
865 (2011).
- 866 [19] G. Bellini et al. (Borexino Collaboration), *Phys. Rev. D* **89**, 112007  
867 (2014).
- 868 [20] F.P. An et al. (Daya Bay Collaboration), [arxiv:1407.0275](https://arxiv.org/abs/1407.0275).
- 869 [21] [http://www.toray.jp/films/en/properties/lumirror/lum\\_e6sr.html](http://www.toray.jp/films/en/properties/lumirror/lum_e6sr.html), archived at [https://web.archive.org/web/20110405061457/http://www.toray.jp/films/en/properties/lumirror/lum\\_e6sr.html](https://web.archive.org/web/20110405061457/http://www.toray.jp/films/en/properties/lumirror/lum_e6sr.html).
- 870 [22] A. Wright, P. Mosteiro, and F. Calaprice, *Nucl. Instr. Meth. A* **644**, 18  
871 (2011).
- 872 [23] L.R. Greenwood and N.R. Chellew, *Rev. Sci. Instr.* **50**, 466 (1979).
- 873 [24] S.C. Wang et al., *Nucl. Instr. Meth. A* **432**, 111 (1999).
- 874 [25] T. Alexander et al. (SCENE Collaboration), *Phys. Rev. D* **88**, 092006  
875 (2013).

- 879 [26] T. Alexander et al. (SCENE Collaboration), [arxiv:1406.4825](https://arxiv.org/abs/1406.4825). Note that  
 880 in Column 2 of our Table ??, we need  $\mathcal{L}_{\text{eff}, 83m\text{Kr}}$  for 200 V/cm, that  
 881 is, the nuclear recoil light yield at 200 V/cm divided by the  $^{83m}\text{Kr}$  at  
 882 zero field. This is not tabulated in the SCENE paper. (Table II of this  
 883 reference gives  $\mathcal{L}_{\text{eff}, 83m\text{Kr}}$  at zero field.) For our Table ??, we use the  
 884 200 V/cm data plotted in Fig. 8 of this reference.
- 885 [27] [www.saesgetters.com](http://www.saesgetters.com), archived at <https://web.archive.org/web/20141222175229/http://www.saesgetters.com/>.
- 887 [28] D. Vénos, A. Špalek, O. Lebeda, M. Fišer, *Appl. Rad. Isotopes* **63**, 323  
 888 (2005).
- 889 [29] W.H. Lippincott, S.B. Cahn, D. Gastler, L.W. Kastens, E. Kearns,  
 890 D.N. McKinsey, and J.A. Nikkel, *Phys. Rev. C* **81**, 045803 (2010).
- 891 [30] S. Kubota, M. Hishida, and A. Nohara, *Nucl. Instr. Meth.* **150**, 561,  
 892 (1978); M.J. Carvalho and G. Klein, *J. Lumin.* **18-19**, 487 (1979);  
 893 J.W. Keto, R.E. Gleason, and F.K. Soley, *J. Chem. Phys.* **71**, 2676  
 894 (1979); T. Suemoto and H. Kanzaki, *J. Phys. Soc. Japan* **46**, 1554  
 895 (1979); S. Kubota, M. Hishida, M. Suzuki, J-z. Ruan, *Nucl. Instr.*  
 896 *Meth.* **196**, 101 (1982); S. Kubota et al., *Phys. Rev. B* **20**, 3486 (1979).
- 897 [31] A. Hitachi, T. Takahashi, N. Funayama, K. Masuda, J. Kikuchi, and  
 898 T. Doke, *Phys. Rev. B* **27**, 5279 (1983).
- 899 [32] E. Shibamura, K. Masuda, and T. Doke, Research Report to the Min-  
 900 istry of Education, Science, Sport, and Culture for Grant-in-Aid Sci-  
 901 entific Research(C), No. 62540284 (1988).
- 902 [33] P. Benetti et al., *Nucl. Instr. Meth. A* **327**, 203 (1993).
- 903 [34] P. Agnes et al. (DarkSide Collaboration), [arxiv:1412.2969](https://arxiv.org/abs/1412.2969).
- 904 [35] [www.caen.it](http://www.caen.it), archived at  
 905 <https://web.archive.org/web/20150104083159/http://www.caen.it/>.
- 907 [36] [www.ni.com](http://www.ni.com), archived at  
 908 <https://web.archive.org/web/20150218101935/http://www.ni.com/>.

- 910 [37] [www.highlandtechnology.com](http://www.highlandtechnology.com), archived at <https://web.archive.org/web/20150215110202/http://www.highlandtechnology.com/>.
- 911
- 912 [38] C. Green et al., *J. Phys. Conf. Ser.* **396**, 022020 (2012).
- 913 [39] A. Empl, R. Jasim, E.V. Hungerford, and P. Mosteiro, *JCAP* **1408**, 64 (2014).
- 914
- 915 [40] T. Pollmann, M. Boulay, and M. Kuzniak, *Nucl. Instrum. Meth. A* **635**, 127 (2011).
- 916
- 917 [41] A. Pocar, *Low Background Techniques and Experimental Challenges for*  
918 *Borexino and its Nylon Vessels*, Ph.D. Dissertation, Princeton University (2003). [search.proquest.com/docview/288218433/abstract](http://search.proquest.com/docview/288218433/abstract).
- 919
- 920 [42] J. Benziger et al., *Nucl. Instr. Meth. A* **582**, 509 (2007).
- 921 [43] B. Aharmim et al. (SNO Collaboration), *Phys. Rev. Lett.* **101**, 111301 (2008).
- 922
- 923 [44] W.H. Lippincott, K. J. Coakley, D. Gastler, A. Hime, E. Kearns,  
924 D.N. McKinsey, J.A. Nikkel, and L.C. Stonehill, *Phys. Rev. C* **78**,  
925 035801 (2008). Note that there is a misprint in the relevant equation  
926 11.
- 927 [45] M.G. Boulay et al. (DEAP Collaboration), [arxiv:0904.2930](http://arxiv.org/abs/0904.2930).
- 928 [46] J.D. Lewin and P. Smith, *Astropart. Phys.* **6**, 87 (1996).
- 929 [47] C. Savage, K. Freese, and P. Gondolo, *Phys. Rev. D* **74**, 043531 (2006).
- 930 [48] M.C. Smith et al., *Mon. Not. Roy. Astron. Soc.* **379**, 755 (2007).
- 931 [49] C. Savage, G. Gelmini, P. Gondolo, and K. Freese, *JCAP* **0904**, 010 (2009).
- 932
- 933 [50] D.S. Akerib et al. (LUX Collaboration), *Phys. Rev. Lett.* **112**, 091303 (2014).
- 934
- 935 [51] E. Aprile et al. (XENON100 Collaboration), *Phys. Rev. Lett.* **109**, 181301 (2012).
- 936
- 937 [52] M. Xiao et al. (PandaX Collaboration), [arxiv:1408.5114](http://arxiv.org/abs/1408.5114).

<sup>938</sup> [53] Z. Ahmed et al. (CDMS II Collaboration), [Science 327, 1619 \(2010\)](#).